Supplementary information

Interfacial strain and defects in asymmetric Fe-Mn oxides hybrid nanoparticles

Arnaud Mayence,[a] Madeleine Wéry,[a] Dung Trung Tran,[a] Erik Wetterskog,[b] Peter Svedlindh,[b] Cheuk-Wai Tai,[a] Lennart Bergström[a]*

[a]Arrhenius Laboratory, Department of Materials and Environmental Chemistry, Stockholm University, Stockholm, Sweden.

[b]Department of Engineering Sciences, Uppsala University, Uppsala, Sweden.

1. TEM analysis of iron oxide nanocubes and Fe-Mn oxides hybrid nanoparticles

a) Iron oxide nanocubes (IOC)

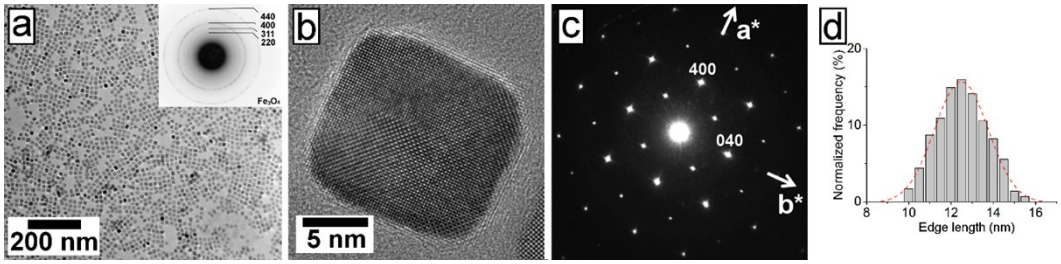

Figure S1. **TEM of iron oxides nanocubes.** (a) TEM image of iron oxide nanocubes, and electron diffraction pattern inset. (b) HRTEM image of an iron oxide nanocube recorded along [001] zone axis. (c) Electron diffraction pattern of the nanocube shown in (b). (d) Histogram of the nanocubes edge length distribution. The solid dashed curve depicts a normal distribution with a size (average edge length, L_{edge}) of 12.5 nm with a standard deviation, σ, of 1.3 nm.

b) Fe-Mn oxides hybrid nanoparticles synthesized using benzyl ether (FeMnO-b)

Statistical analysis was performed on more than 250 isolated Fe-Mn oxides nanoparticles (FeMnO-b). The synthesis yield is as high as 91% and resulted in 41% of dimers, 35% of trimers, and 15% of more complex morphologies. Only 9% of IOC are free of overgrown $Mn_{1-X}O$ phase.

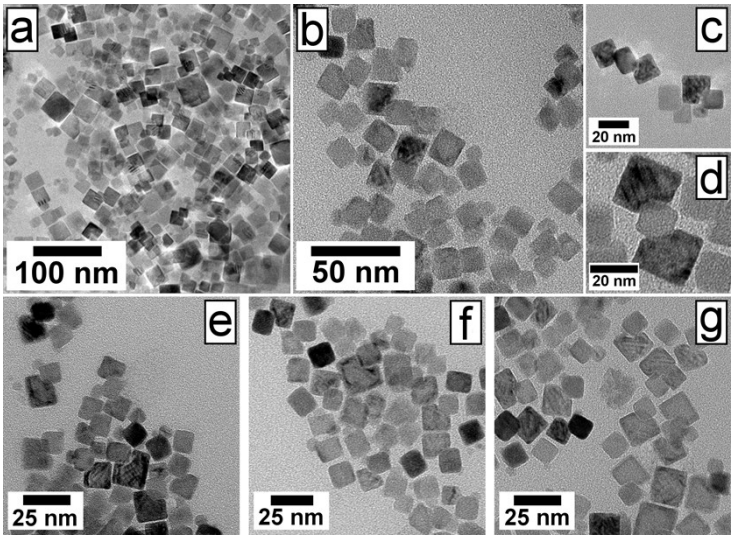

Figure S2. **TEM images of Fe-Mn oxides hybrid nanoparticles synthesized using benzyl ether as solvent.** (a-b and e-g) TEM images of FeMnO-b nanoparticles. (c-d) TEM images of FeMnO-b showing different geometrical configurations of FeMnO-b trimers.

c) Fe-Mn oxides hybrid nanoparticles synthesized using 1-octadecene (FeMnO-o)

FeMnO-o nanoparticles shown in Fig. S3 consist of a $Mn_{1-x}O$ phase grown onto the iron oxides nanocube seeds yielding large nanoparticles. These nanoparticles exhibit no sharp facets unlike the FeMnO-b nanoparticles shown in Fig. S2. The nanoparticle FeMnO-b shown in Fig. S3e does not reveal any particular faceting although this particle is oriented along [001] zone axis. The electron diffraction pattern of the large individual FeMnO-o hybrid nanoparticle shown in Fig. S3f reveals that the nanoparticle consists of a single domain nanocrystal. The Fourier filtered images performed on a small FeMnO-o hybrid nanoparticle (Fig. S4) reveal that the core consists of iron oxides nanocube (i.e. Fourier filtered image using 004_S reflection of iron oxide) and the shell is the $Mn_{1-x}O$ phase (i.e Fourier filtered image using 002_{R-S} reflection of manganese oxide).

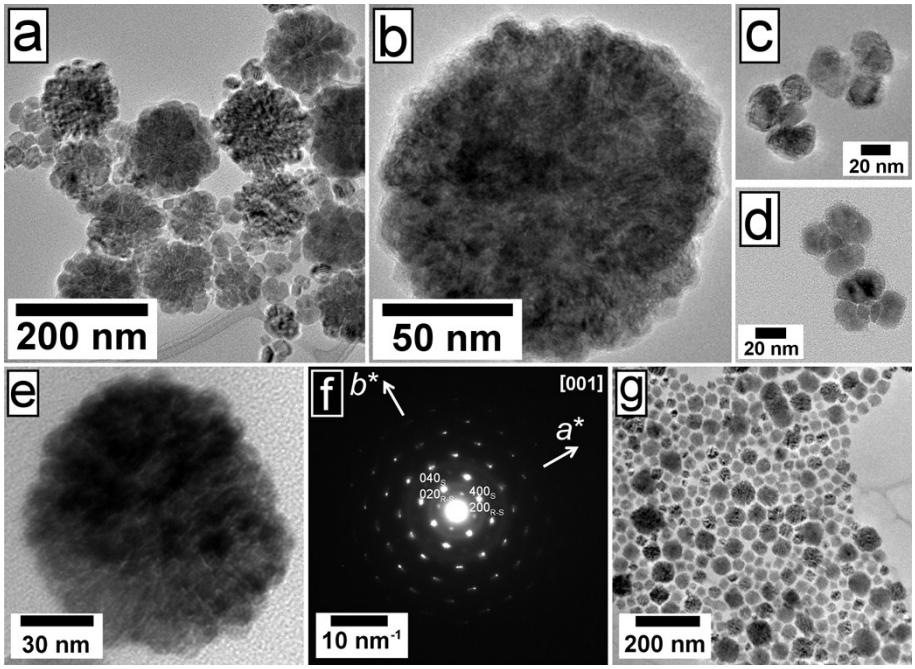

Figure S3. **TEM images of Fe-Mn oxides hybrid nanoparticles synthesized using 1-octadecene as solvent.** (a) Low magnification TEM images of FeMnO-o nanoparticles. (b) TEM image recorded at higher magnification showing a single FeMnO-o nanoparticle. (c-d) TEM image of small FeMnO-o nanoparticles. (e) Individual FeMnO-o nanoparticle. (f) Electron diffraction pattern recorded along a <001> zone axis of the FeMnO-o nanoparticle shown in (e). (g) Low magnification TEM image of FeMnO-o nanoparticles.

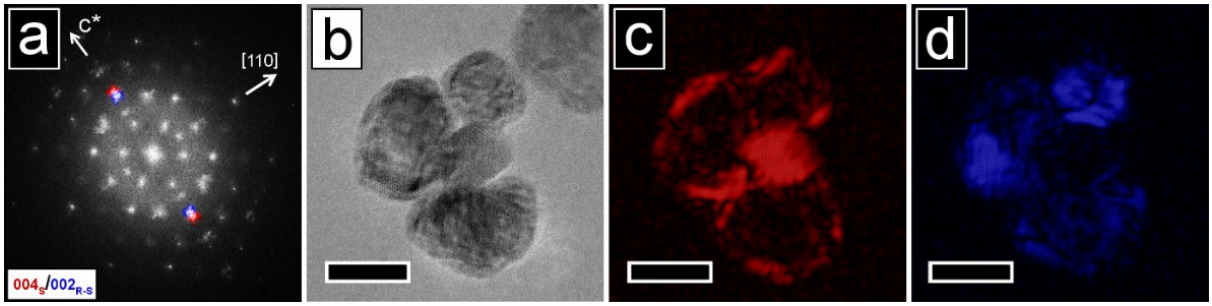

Figure S4. **TEM analysis of a small FeMnO-o nanoparticle**. (a) Fourier transform of (b) TEM image of a small FeMnO-o nanoparticle. (c-d) Fourier filtered images using (c) 004_S and (d) 002_{R-S} reflections highlighted in red and blue in (a), respectively. Scale bars: 20 nm.

2. Powder X-ray diffraction

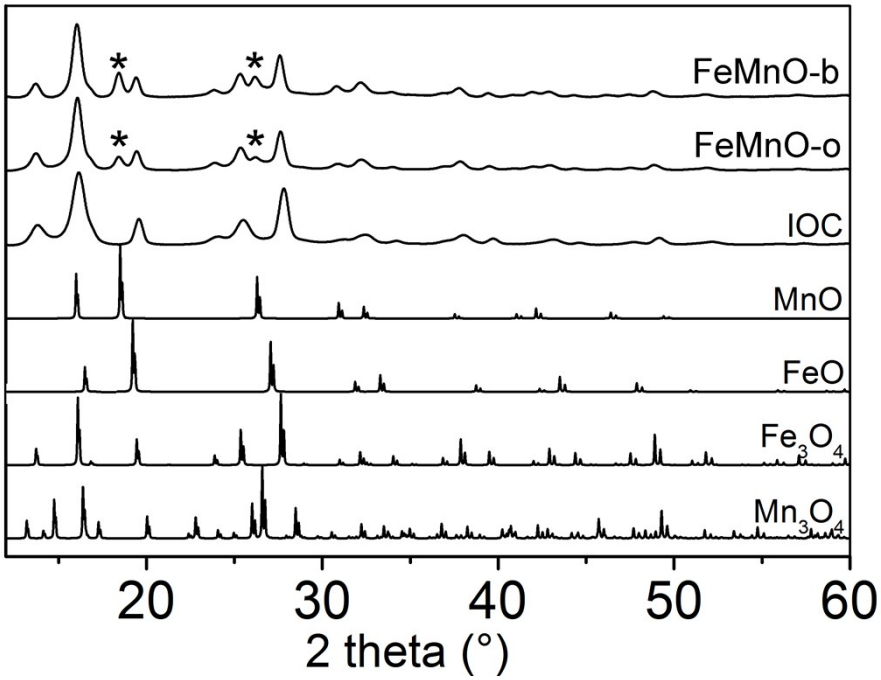

Figure S5. Powder X-ray diffraction patterns of IOC, FeMnO-b, FeMnO-o, and simulated diffraction patterns of FeO, Fe_3O_4, MnO, and Mn_3O_4 phases.

The simulated X-ray diffraction patterns were found on the PDF ICDD database and used as references for experimental peak identification:

- MnO (*a* = 4.40 Å, *Fm*-3*m* (225), PDF ICDD 01-071-4748)

- FeO (*a* = 4.33 Å, *Fm*-3*m* (225), PDF ICDD 01-089-0687)

- Fe_3O_4 (*a* = 8.40 Å, *Fd*-3*m* (227), PDF ICDD 01-072-2303)

- Mn_3O_4 (*a* = 5.76 Å, *c* = 9.439Å, $I4_1/amd$ (141), PDF ICDD 01-075-1560)

The experimental powder X-ray diffraction pattern of IOC shown in Fig. S5 is consistent with Fe_3O_4 although the presence of FeO phase cannot be ruled out. The peaks indexed with a star indicate the presence of MnO phase in the Fe-MnO powders when using either 1-octadecene or benzyl ether as a solvent.

3. EELS and EFTEM elemental mapping

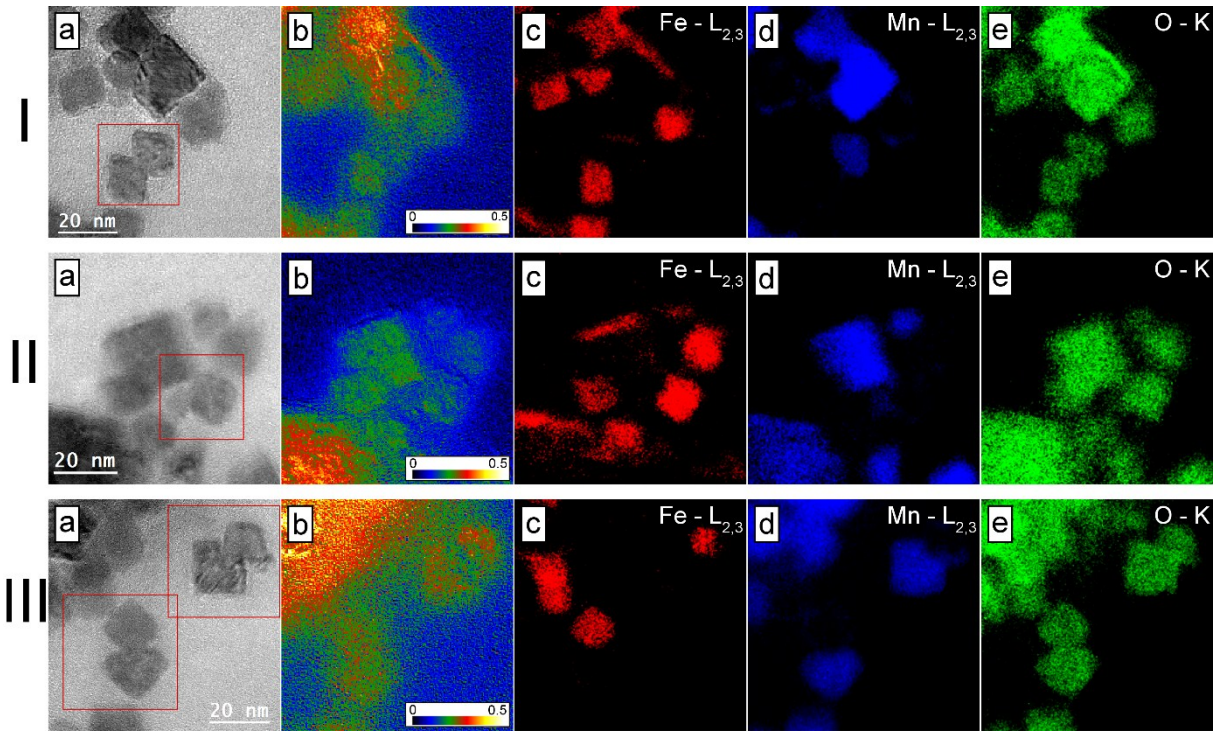

Figure S6. **Elemental mappings of FeMnO-b nanoparticles obtained by EFTEM**. I,II and III-(a) Low-magnification unfiltered TEM images. (b) Thickness maps and (c-e) EFTEM elemental mappings of (c) iron and (d) manganese $L_{2,3}$, and (e) oxygen K edges.

The electron energy loss spectra displayed in Figures S7 and 8 show the O-K, Mn-$L_{2,3}$ and Fe-$L_{2,3}$ edges with a dispersion of 0.2eV/channel, obtained after multiple scattering removal and background subtraction over the edge of interest with 40 eV background fit interval. Each EELS spectrum was acquired with 60 seconds acquisition time. In order to have good signal-to-noise ratio and to minimize the multiple scattering events, the value of the inelastic mean free path, $\lambda_{inelastic}$ was smaller than 1, e.g. 0.62 for FeMnO-b, and 0.58 for IOC. The oxidation states of Fe and Mn were assessed by measuring L_3/L_2 intensity ratios using a double arctan continuum model $L_{2,3}$ edges of IOC and MnO, together with the double-arctan continuum for quantification. The L_3/L_2 ratios of MnO and IOC are shown in Table S1. Energy loss near edge spectroscopy (ELNES) data on branching energy difference $\Delta E_{(L2-L3)}$ and total integral intensity ratio (L_3/ L_2) are correlated to the oxidation state of iron and manganese ions present in the material.[1] Both the L_3/ L_2 ratio (3.89±0.01) and $\Delta E_{(L2-L3)}$ (11.5) of MnO are in good agreement with the values previously found for MnO.[1] The L_3/ L_2 ratio (4.86±0.01) indicates that the nanoparticles composition is between FeO and Fe_3O_4.[2,3]

Table S1. L_3/L_2 white-line ratios measured for MnFeO-b and IOC.

Mn, L_{23} (FeMnO-b)				**Fe, L_{23} (IOC)**			
Integration window (eV)	**L_3 integration (counts)**	**L_2 integration (counts)**	**L_3/L_2 ratio**	**Integration window (eV)**	**L_3 integration (counts)**	**L_2 integration (counts)**	**L_3/L_2 ratio**
6.5	297229	76754	3.87	7.0	916032	188030	4.87
6.75	300900	77451	3.89	7.5	932042	192162	4.85
7.0	303931	77623	3.91	8.0	941707	193572	4.86
Average ratio	**3.89±0.02**			**Average ratio**	**4.86±0.01**		

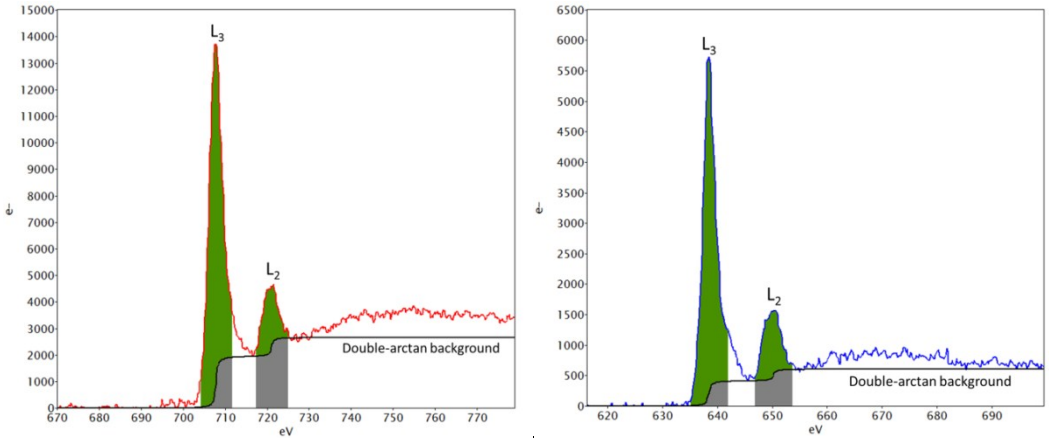

Figure S7. EEL spectra showing $L_{2,3}$ edges and intensity integration based on double-arctan continuum background: (a) Fe-$L_{2,3}$ of IOC and (b) Mn-$L_{2,3}$ of MnFeO-b dimers edges.

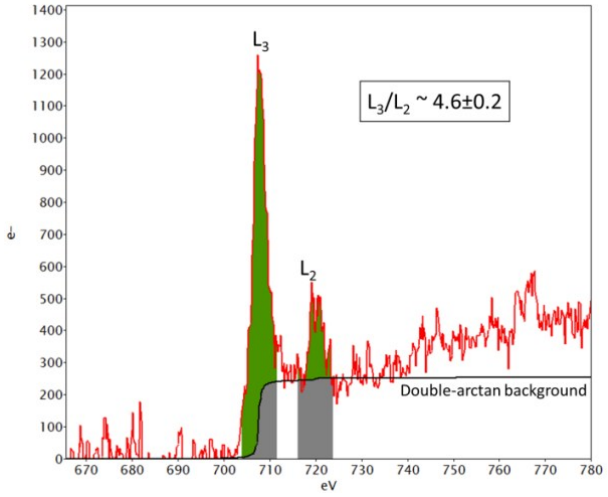

Figure S8. EEL spectrum showing $L_{2,3}$ edges and intensity integration based on double-arctan continuum background: Fe-$L_{2,3}$ edges of MnFeO-b dimers.

Attempts on intensity integration based on double-arctan continuum background were made with an integration window of 7.5 eV for Fe-$L_{2,3}$ of MnFeO-b dimers edges (Fig. S8). However, the data is noisy so there is considerable uncertainty for the measured L_3/L_2 ratio (~4.6). From the pre-edge residual noise, the deviation could be estimated to ~0.2.

4. Magnetization vs Temperature of IOC and FeMnO nanoparticles

The temperature-dependent magnetization curves shown in Fig. S9a suggest that the blocking temperature (T_B) of the IOC is ~200 K. The small deviation in both the ZFC and FC curves at ~185 K is probably stemming from the antiferromagnetic $Fe_{1-x}O$ phase in the IOC core (for bulk FeO, T_N = 203-211 K).[4] The small exchange bias observed in the IOC (H_e = 119 Oe) corroborates the presence of antiferromagnetic $Fe_{1-x}O$. The absence of features around 110-120 K in the ZFC curve (Fig. 9a) indicates that Verwey transition is absent or very small. The curves in Figure S9b display no evidence of the characteristic transition of bulk MnO (T_N = 119 K). The transition at ~90 K may reflect a suppression of the T_N of $Mn_{1-x}O$ due to defects or finite size effects. In fact, alterations of the T_N of $Mn_{1-x}O$ due to finite size effects have been observed previously, but only in the opposite direction.[5] The blocking temperature of FeMnO-b could not be determined because of organic impurities present in the sample (Fig. S9c).

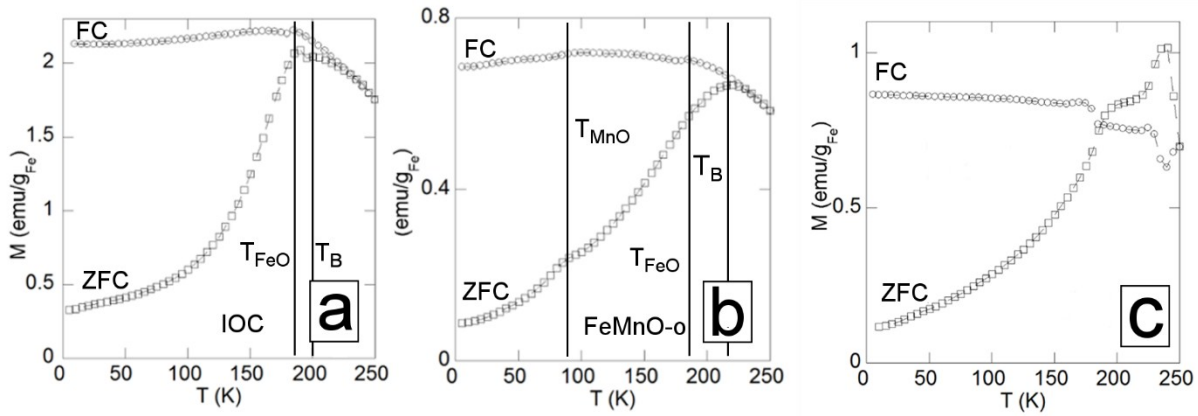

Figure S9. **Temperature dependence of the magnetization of iron oxides nanocubes (IOC) iron-manganese oxides hybrid nanoparticles (FeMnO-b and FeMnO-o).** (a, b and c) Temperature dependence of the magnetization of IOC (a) and FeMnO-o (b) and FeMnO-b (c) nanomaterials. The FC measurements were performed using an applied field of 5 Oe.

References

1 H. K. Schmid and W. Mader, *Micron*, 2006, **37**, 426–432.

2 P. A. van Aken and B. Liebscher, *Phys. Chem. Miner.*, 2002, **29**, 188–200.

3 C. Colliex, T. Manoubi and C. Ortiz, *Phys. Rev. B*, 1991, **44**, 11402–11411.

4 V. Skumryev, S. Stoyanov, Y. Zhang, G. Hadjipanayis, D. Givord and J. Nogués, *Nature*, 2003, **423**, 850–853.

5 I. V. Golosovsky, I. Mirebeau, V. P. Sakhnenko, D. A. Kurdyukov and Y. A. Kumzerov, *Phys. Rev. B*, 2005, **72**, 144409.